DIRECT SIMULATION OF EVOLUTION AND CONTROL OF NONLINEAR INSTABILITIES IN ATTACHMENT–LINE BOUNDARY LAYERS

Ronald D. Joslin*
NASA Langley Research Center
Hampton, Virginia 23681-0001

Abstract

The unsteady, incompressible Navier-Stokes equations are used for the direct numerical simulation (DNS) of spatially evolving disturbances in a three-dimensional (3-D) attachment-line boundary layer. Two-dimensional (2-D) disturbances are introduced either by forcing at the inflow or by harmonic-source generators at the wall; 3-D disturbances are introduced by harmonic-source generators at the wall. The DNS results are in good agreement with both 2-D nonparallel theory (for small-amplitude disturbances) and weakly nonlinear theory (for finite-amplitude disturbances), which validates the two theories. The 2-D DNS results indicate that nonlinear disturbance growth occurs near branch II of the neutral stability curve; however, steady suction can be used to stabilize this disturbance growth. For 3-D instabilities that are generated off the attachment line, spreading both toward and away from the attachment line causes energy transfer to the attachment-line and downstream instabilities; suction stabilizes these instabilities. Furthermore, 3-D instabilities are more stable than 2-D or quasi-2-D instabilities.

1. Introduction

Many instability mechanisms can occur that cause the breakdown from laminar to turbulent flow on swept wings; however, this discussion will focus on only those disturbances that evolve near the attachment-line region (near the leading edge). Turbulent contamination, which results from turbulence at a fuselage-wing juncture, can travel out over the wing and cause laminar flow on the wing to become turbulent. To prevent this contamination, devices such as the Gaster bump[1] or suction (Pfenninger[2]), implemented near the wing root, can halt the turbulent attachment-line boundary layer from sweeping out over the entire wing.

Although the problem of turbulent flow that originates from the fuselage-wing juncture can be avoided with a device such as the Gaster bump, a Reynolds number must exist beyond which disturbances generated by surface imperfections or particulates on the wing, coupled with noise, eventually cause transition. If we assume that the initiated disturbances are sufficiently small, then hydrodynamic stability theory could potentially be used to predict the spatial amplification and decay of the disturbances along the attachment line. Gaster[3] first examined this small-amplitude disturbance problem by using acoustic excitation along the attachment line of a swept-cylinder model. Gaster generated sine waves with various frequencies that were detected in the flow by a hot-film gauge on the attachment line. He noted that the recorded oscillations had preferred frequency bands that changed with tunnel speed and that this behavior was reminiscent of traveling-wave instabilities. From his measurements, he concluded that the small-amplitude disturbances in an attachment-line boundary layer were stable for momentum-thickness Reynolds numbers R_θ below 170 (the critical Reynolds number was outside the experimental range). This value for the critical Reynolds number is close to the theoretical value of 200, which is obtained by assuming a two-dimensional (2-D) attachment-line boundary layer. Later, Cumpsty and Head[4] experimentally studied large-amplitude disturbances and turbulent flow along the attachment line of a swept-wing model. Without tripping the boundary-layer instabilities, they observed that laminar flow is stable to small-amplitude disturbances up to $R_\theta \simeq 245$ (which corresponds to the top speed of the tunnel). They note that this observation does not contradict the theoretical value; an accurate theoretical value would need to account for three-dimensional (3-D) effects. At the same time, Pfenninger and Bacon[5] used a wing swept to 45° to experimentally study the attachment-line instabilities in a wind tunnel that could reach speeds large enough to obtain unstable disturbances. With hot wires, they observed regular sinusoidal oscillations with frequencies comparable to the most unstable 2-D modes of theory; these modes caused transition at about $R_\theta \simeq 240$. A continued interest in the transition initiated near the attachment line of swept wings led Poll[6,7] to perform additional experiments with the swept circular model of Cumpsty and Head[4]. Like Pfenninger and Bacon[5], Poll observed disturbances that amplified along the attachment line. He noted that no unstable modes were observed below $R_\theta = 230$.

With nonparallel stability theory, Hall et al.[8] studied the linear stability of the attachment-line boundary-layer flow called swept Hiemenz flow, which is sketched

*Research Scientist, Theoretical Flow Physics Branch, Member AIAA

in Fig. 1. This 3-D base flow is an exact solution of the Navier-Stokes equations; hence, its use is advantageous in stability analyses. By assuming 2-D instability modes, Hall et al.[8] demonstrated that the attachment-line boundary layer can theoretically be stabilized with small amounts of suction. Hall and Malik[9] extended this theory to account for weakly nonlinear stability. They note that subcritical instability is observed at wave numbers that correspond to the upper branch of the neutral curve. The neutral curve and the subcritical instability region of Hall and Malik[9] are shown in Fig. 2 with the experimental results of Pfenninger and Bacon[5] and Poll.[6,7] Consistent with the Pfenninger and Bacon[5] experimental results, large-amplitude disturbances became unstable before the linear critical point.

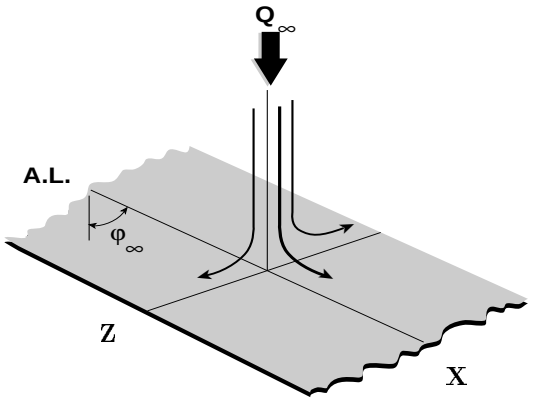

Fig. 1. Sketch of attachment-line region of swept Hiemenz flow.

Hall and Seddougui[10] studied oblique waves and their interaction in attachment-line flow at the large Reynolds number limit. They note that close to the attachment line a small band of destabilized oblique modes appears, interacts with the 2-D mode, and causes a breakdown of the 2-D mode. Further, they note that oblique modes become less important further away from the attachment line and that low-frequency modes become the dominant mechanism. (Perhaps stationary crossflow modes arise near and dominate away from the attachment line.)

Finally, Spalart[11] used a direct numerical simulation (DNS) approach, based on the fringe method, to study the leading-edge contamination problem. Small-amplitude disturbances were initialized with white noise. A Reynolds number range with a width of 50 was selected. At the lower Reynolds number, all disturbances decayed; at the higher number, at least one mode was amplified. The neutral curve predicted by Hall et al.[8] fell within the Reynolds number range used by Spalart. These results show qualitative agreement with the linear theory of Hall et al.[8] Furthermore, Spalart[11] demonstrated that simple Hiemenz flow (i.e., $R = 0$) is both linearly and nonlinearly stable.

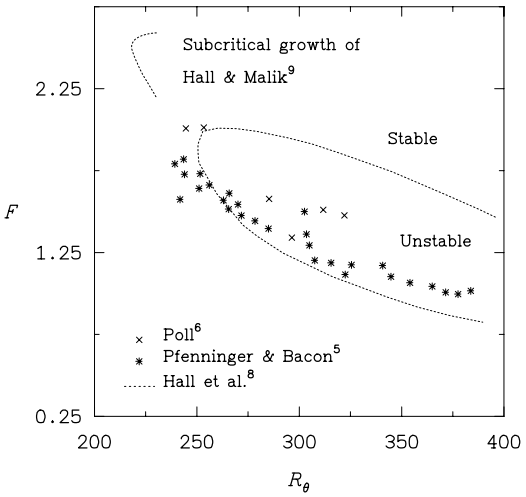

Fig. 2. Neutral curve, experimental regions of instability growth, and theoretical region of subcritical growth in attachment-line boundary layer.

For the present study, a 2-D spatial DNS code described by Joslin et al.[12,13] and a newly developed 3-D spatial DNS code described in this paper are used to study the linear and nonlinear instabilities that initiate and develop along the attachment line of swept Hiemenz flow. The region near branch II of the neutral curve is investigated with DNS to verify the nonparallel theory of Hall et al.[8] for infinitesimal disturbances. Subcritical instability growth in the region shown in Fig. 2 was predicted with the weakly nonlinear theory of Hall and Malik;[9] however, recent DNS results by both Jiménez et al.[14] and Theofilis[15] failed to find this subcritical growth. Jiménez et al.[14] contend that this subcritical growth region does not exist. Here, an independent study is conducted to determine if nonlinearly growing disturbances can be found. Furthermore, because the true physical problem involves 3-D disturbances that may be on or off the attachment line, 3-D simulations are conducted to determine the importance of 3-D disturbances near the attachment line. Steady suction is used to control instability growth.

2. Problem Formulation

For the problem at hand, the velocities $\underline{\tilde{u}} = (\tilde{u}, \tilde{v}, \tilde{w})$ and the pressure $\tilde{p}$ are solutions of the incompressible, unsteady Navier-Stokes equations. The instantaneous velocities $\underline{\tilde{u}}$ and the pressure $\tilde{p}$ may be decomposed into base and disturbance components as

$$\{\underline{\tilde{u}}, \tilde{p}\}(\underline{x}, t) = \{\underline{U}, P\}(\underline{x}) + \{\underline{u}, p\}(\underline{x}, t) \tag{1}$$

The base flow is given by the velocities $\underline{U} = (U, V, W)$ and the pressure P; the disturbance component is given by the velocities $\underline{u} = (u, v, w)$ and the pressure p. A Cartesian coordinate system $\underline{x} = (x, y, z)$ is used, in which x is aligned with the attachment line, y is wall normal, and z corresponds to the direction of flow acceleration away from the attachment line.

Originally described by Hall et al.[8], the base flow referred to as a swept Hiemenz flow is an exact solution to the incompressible 3-D Navier-Stokes equations. The velocities at the wall are

$$U = W = 0 \quad \text{and} \quad V = V_o \qquad \text{at} \quad y = 0 \tag{2}$$

Away from the wall, the velocities are

$$U \to U_o \quad \text{and} \quad W \to W_o \frac{z}{L} \qquad \text{as} \qquad y \to \infty \tag{3}$$

where U_o, V_o, W_o are independent velocity scales and L is the length scale in the flow-acceleration direction z. Shown in Fig. 1, the fluid comes straight down toward the wall; it turns away from the attachment line into the $\pm z$ directions to form a boundary layer. In the x direction, the flow is uniform. In the absence of sweep, U_o is equal to 0, and the flow reduces to the 2-D stagnation flow first described by Hiemenz.[16] A boundary-layer thickness is defined in the yz-plane as $\delta = \sqrt{\nu L / W_o}$; a Reynolds number, as $R = U_o \delta / \nu = 2.475 R_\theta$; and a transpiration constant, as $\kappa = V_o \sqrt{L / \nu W_o}$, where $\kappa = 0$ for the zero-suction case. If the attachment line is assumed to be infinitely long, the velocities become functions of z and y only, and an exact solution of the Navier-Stokes equations can be found.

In accordance with Hall et al.,[8] the equations for the base flow are

$$\hat{W} + \hat{V}_Y = 0 \tag{4}$$

$$\hat{V}_{YYY} + \hat{V}_Y^2 - \hat{V}\hat{V}_{YY} - 1 = 0 \tag{5}$$

$$\hat{U}_{YY} - \hat{V}\hat{U}_Y = 0 \tag{6}$$

where $\{X, Y, Z\} = \{x, y, z\}/\delta$, the subscript Y denotes derivatives with respect to Y, and the hats refer to similarity variables. The boundary conditions are given by

$$\hat{V}_Y = 0, \qquad \hat{V} = \kappa, \quad \text{and} \quad \hat{U} = 0 \quad \text{at} \quad Y = 0 \tag{7}$$

$$\hat{V}_Y \to -1 \quad \text{and} \quad \hat{U} \to 1 \quad \text{as} \quad Y \to \infty \tag{8}$$

If the solutions of equations (4)-(8) are nondimensionalized with respect to the attachment-line velocity U_o, the boundary-layer thickness δ, and the kinematic viscosity ν, then the base flow is

$$U(Y) = \hat{U}(Y), \; V(Y) = \frac{1}{R}\hat{V}(Y), \; W(Y, Z) = \frac{Z}{R}\hat{W}(Y) \tag{9}$$

For the disturbance portion of equation (1), the 3-D incompressible Navier-Stokes equations are solved in disturbance form as

$$\frac{\partial \underline{u}}{\partial t} + (\underline{u} \cdot \nabla)\underline{u} + (\underline{U} \cdot \nabla)\underline{u} + (\underline{u} \cdot \nabla)\underline{U} = -\Delta p + \frac{1}{R}\nabla^2 \underline{u} \tag{10}$$

with the continuity equation

$$\nabla \cdot \underline{u} = 0 \tag{11}$$

and boundary conditions

$$\underline{u} = 0 \;\text{ at }\; Y = 0 \quad \text{and} \quad \underline{u} \to 0 \;\text{ as }\; Y \to \infty \tag{12}$$

Disturbances are forced either at the inflow or by harmonic-source generators, which use suction and blowing at the wall and are assumed to decay to zero in the far field. At the inflow, solutions of the base flow are forced, and the buffer-domain technique is employed as the outflow condition.

3. Numerical Methods of Solution

In the attachment-line (X) direction, discretization is accomplished with fourth-order central finite differences for the pressure equation and sixth-order compact differences for the momentum equations in the interior of the computational domain. At the boundary and near-boundary nodes, fourth-order forward and backward differences are used. The discretization yields a pentadiagonal system for the finite-difference scheme and a tridiagonal system for the compact-difference scheme. The approximations can be solved efficiently by appropriate backward and forward substitutions.

In both the wall-normal (Y) and flow-acceleration (Z) directions, Chebyshev series are used to approximate the disturbances at Gauss-Lobatto collocation points. A Chebyshev series is used in the wall-normal direction to provide good resolution in the high-gradient regions near the boundaries. Furthermore, the use of as few grid points as possible results in significant computational cost savings. In particular, the use of the Chebyshev series enables an efficient pressure solver. Because this series and its associated spectral operators

are defined on [-1, 1] and because the physical problem of interest has a truncated domain $[0, y_{\max}]$ and $[-z_{\max}, z_{\max}]$, transformations are employed. Furthermore, stretching functions are used to cluster the grid near both the wall and the attachment line. For further details on the properties and the use of spectral methods, refer to Canuto et al.[17]

For time marching, a time-splitting procedure was used with implicit Crank-Nicolson differencing for normal diffusion terms; an explicit three-stage Runge-Kutta (RK) method was used for the remaining terms. The pressure is omitted from the momentum equations (10) for the fractional RK stage, which leads to

$$\frac{\partial \underline{u}^*}{\partial t} + (\underline{u}^* \cdot \nabla)\underline{u}^* + (\underline{U} \cdot \nabla)\underline{u}^* + (\underline{u}^* \cdot \nabla)\underline{U} = \frac{1}{R}\nabla^2 \underline{u}^* \quad (13a)$$

$$\underline{u}^*_\tau = \underline{u}_{BC} + h_t^m \left[(1 + \frac{h_t^m}{h_t^{m-1}})\nabla p_\tau^m - \frac{h_t^m}{h_t^{m-1}} \nabla p_\tau^{m-1} \right] \quad (13b)$$

where h_t^m are time-step sizes in the RK scheme, time is advanced from $\underline{u}^m$ to the intermediate disturbance velocities $\underline{u}^*$, and $\underline{u}^*_\tau$ are intermediate boundary conditions described by Joslin et al.[12] to reduce the time-marching slip velocities that may arise. For the boundary conditions, $\underline{u}_{BC} = 0$ for a rigid wall and $\underline{u}_{BC} = \underline{u}_o$ for an inflow condition or a wall-slot condition evaluated at the appropriate time in the RK stage.

A full RK stage is completed by advancing the solution in time from $\underline{u}^*$ to $\underline{u}^{m+1}$ by

$$\frac{\partial \underline{u}}{\partial t}^{m+1} = -\nabla p^{m+1} \quad (14a)$$

$$\nabla \cdot \underline{u}^{m+1} = 0 \quad (14b)$$

If the divergence of equation (14a) is taken and zero divergence of the flow field is imposed at each RK stage, then a pressure equation is obtained:

$$\nabla^2 p^{m+1} = \frac{1}{h_t^m}(\nabla \cdot \underline{u}^*) \quad (15)$$

which is subject to homogeneous Neumann boundary conditions. This boundary condition is justified in the context of a time-splitting scheme as discussed by Streett and Hussaini.[18]

The solution is determined on a staggered grid. The intermediate RK velocities ($\underline{u}^*$) are determined by solving equation (13) on Gauss-Lobatto points. The pressure (p^{m+1}) is found by solving equation (15) on Gauss points and is then spectrally interpolated onto Gauss-Lobatto points. Then, the full RK stage velocities ($\underline{u}^{m+1}$) are obtained from equation (14) on Gauss-Lobatto points. The above system is solved three consecutive times to obtain full time-step velocities. The three-stage RK time steps given by Williamson[19] are $\{h_t^1, h_t^2, h_t^3\} = \{1/3, 5/12, 1/4\}h_t$, where the sum of the three RK time stages equals the full time step (h_t).

To satisfy global mass conservation, an influence-matrix method is employed and is described in some detail by Streett and Hussaini,[18] Danabasoglu, Biringen, and Streett;[20,21] and Joslin et al.[12,13] For boundary-layer flow, four Poisson-Dirichlet problems are solved for the discrete mode that corresponds to the zero eigenvalue of the system; single Poisson-Neumann problems are solved for all other modes. To efficiently solve the resulting Poisson problem given by equation (15), the tensor-product method of Lynch et al.[22] is used. The discretized form of equation (15) is

$$\Big(L_x \otimes I \otimes I + I \otimes L_y \otimes I + I \otimes I \otimes L_z\Big)p = R \quad (16)$$

where p is the desired pressure solution; R is the right side of equation (15); I is the identity matrix; L_x is the attachment-line-directed central finite-difference operator; L_y and L_z are the wall-normal-directed and flow-acceleration-directed spectral operators; and $\otimes$ infers a tensor product. By decomposing the operators L_y and L_z into their respective eigenvalues and eigenvectors, we find

$$L_y = Q\Lambda_y Q^{-1} \qquad \text{and} \qquad L_z = S\Lambda_z S^{-1} \quad (17)$$

where Q and S are the eigenvectors of L_y and L_z, Q^{-1} and S^{-1} are inverse matrices of Q and S, and Λ_y and Λ_z are the eigenvalues of L_y and L_z. The solution procedure reduces to the following sequence of operations to determine the pressure p:

$$\begin{aligned} p^* &= (I \otimes Q^{-1} \otimes S^{-1})R \\ p^\dagger &= (L_x \otimes I \otimes I + I \otimes \Lambda_y \otimes I + I \otimes I \otimes \Lambda_z)^{-1} p^* \\ p &= (I \otimes Q \otimes S)p^\dagger \end{aligned} \quad (18)$$

Because the number of grid points in the attachment-line direction is typically an order of magnitude larger than the wall-normal and flow-acceleration directions, the operator L_x is much larger than both L_y and L_z. Because L_x is large and has a sparse pentadiagonal structure and because Λ_y and Λ_z influence the diagonal only, an LU decomposition is performed for the second stage of equation (18) once, and forward and backward solves are performed for each time step of the simulation. The first and third steps of the pressure solve for equation (18) involve matrix multiplications.

To obtain the attachment-line-directed operator L_x, central finite differences are used. To find the wall-normal L_y and flow-acceleration L_z operators, the following matrix operations are required:

$$L_y = I_{GL}^G D_y \tilde{D}_y I_G^{GL} \qquad \text{and} \qquad L_z = I_{GL}^G D_z \tilde{D}_z I_G^{GL} \quad (19)$$

where D_y is a spectral, wall-normal derivative operator for the stretched grid; D_z is the spectral, derivative operator that is grid clustered in the attachment-line region; and $\tilde{D}_y$ and $\tilde{D}_z$ are the derivative operators with the first and last rows set to 0. The interpolation matrix I^G_{GL} operates on variables at Gauss-Lobatto points and transforms them to Gauss points; the interpolation matrix I^{GL}_G performs the inverse operation. The spectral operators are described in detail by Canuto et al.[17] and Joslin et al.[13]

The operators $\{L_x, L_y, L_z\}$, the eigenvalue matrices $\{\Lambda_y, \Lambda_z\}$, the eigenvector matrices $\{Q, Q^{-1}, S, S^{-1}\}$, and the influence matrix are all mesh-dependent matrices and must be calculated only once.

The buffer-domain technique introduced by Streett and Macaraeg[23] is used for the outflow condition. As shown by Joslin et al.[12] for the flat-plate boundary-layer problem, a buffer length of three disturbance wavelengths is adequate for traveling waves. The disturbances are assumed to be from the discrete spectrum, which exponentially decays with distance from the wall. Both at the wall and in the far field, homogeneous Dirichlet conditions are imposed. For 3-D simulations, both homogeneous Dirichlet and Neumann conditions have been used in the flow-accelerated direction. With either condition, the disturbance will develop in the same manner along the attachment line, provided that the boundaries are sufficiently far from the attachment-line region. The base flow is used for the inflow boundary condition. Finally, disturbances are forced by unsteady suction and blowing of the wall-normal velocity component through the wall (harmonic-source generators). Although the disturbances may be generated by random frequency input, the disturbances of interest here are forced with known frequencies.

4. Two-Dimensional Simulation Results

The simulations are performed on a grid of 661 points ($\simeq$ 60 points per wavelength) along the attachment line and 81 points in the wall-normal direction. The far-field boundary is located at 50δ from the wall, and the computational length along the attachment line is 216.56δ. For the time-marching scheme, the disturbance wavelength was divided into 320 time steps per period for small-amplitude disturbances and into 2560 time steps for large-amplitude disturbances (stability considerations). The total Cray Y-MP time for a simulation with a single processor was 1.5 hrs for small-amplitude disturbances and 11 hrs for large-amplitude disturbances.

4.1 Subcritical Growth

Recall that Hall and Malik[9] developed a weakly nonlinear theory to predict the growth and decay of instabilities in the attachment-line boundary-layer flow. With swept Hiemenz flow, they discovered regions where 2-D disturbances encountered subcritical growth; however, the linear theory predicted stable modes. Later, both Jiménez et al.[14] and Theofilis[15] discounted this discovery with recently developed 2-D DNS codes. To resolve this discrepancy, the results from the present study of attachment-line boundary-layer disturbances in swept Hiemenz flow (computed with a well-tested spatial DNS code) are compared with the previous studies of Hall et al.[8], Hall and Malik[9], Jiménez et al.[14], and Theofilis.[15] In addition, the effects of suction on unstable modes are documented.

Disturbances for the first simulations are forced at the computational inflow with an amplitude of $A = 0.001$ percent (i.e., some small amplitude), to compare the DNS results with linear stability theory (LST). The Reynolds number $R = 570$ and the frequency $\omega = 0.1249$ correspond to the region of subcritical growth found by Hall and Malik[9], in which disturbances are linearly stable. Disturbances that evolve in both a base flow that complements the quasi-parallel LST assumptions ($V = 0$) and the full, swept Hiemenz flow are computed with DNS. The computed disturbance decay rate and the wavelength in the quasi-parallel flow agree with LST. The disturbance that propagates in the complete swept Hiemenz flow closely retains the wavelength predicted by LST, but decays at a slower rate than that predicted by LST. This change in decay rate is consistent with the theory of Hall et al.[8] From this comparison, we find that the wall-normal velocity (V) terms in the stability equations have a destabilizing effect on the disturbance.

The fundamental wave, the mean-flow distortion, and the harmonics from a simulation forced at the inflow with a large amplitude of $A = 12$ percent, a Reynolds number of $R = 570$, and a frequency of $\omega = 0.1249$ are shown in Fig. 3. After a transient region of adjustment, the fundamental wave encounters subcritical growth, which is in agreement with the weakly nonlinear theory of Hall and Malik.[9] Because DNS involves many parameters (e.g., grid, time-step size, order of methods), the potential for errors was high in the work of Jiménez et al.;[14] erroneous results may have misled them to refute the concept of subcritical growth. For this flow, instantaneous and mean attachment-line and wall-normal velocity profiles at various attachment-line locations are shown in Fig. 4. The profiles indicate that time-dependent distortions to the base flow are observed, but the mean flow ($U + u_o$), which consists of the base flow and the mean-flow distortion components, shows little deviation from the base-flow solution. However, both the time-dependent and mean wall-normal

profiles undergo distortions because of the disturbance. Finally, Fig. 5 shows the wall-normal component of the base flow that corresponds to $R = 570$ and $R = 670$. A comparison of these base-flow profiles with the mean flow of Fig. 4 shows that a large-amplitude disturbance produces a distortion to the base flow, which causes an effective increase in the base Reynolds number. The increase in Reynolds number alone does not account for the growing mode (based on linear stability analysis with the same frequency). However, we surmise that (similar to nonparallel effects) nonlinear disturbances broaden the neutral curve toward higher frequencies in the critical region.

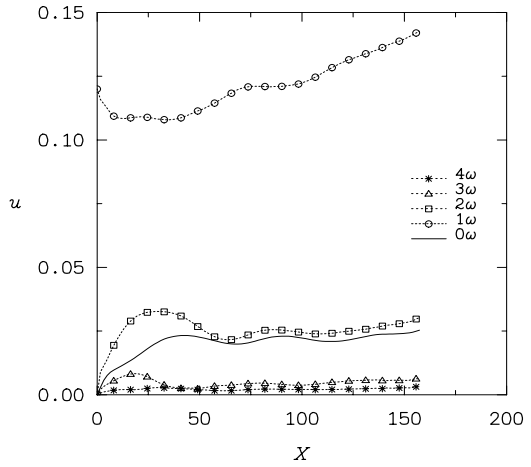

Fig. 3. Nonlinear subcritical disturbance growth in attachment-line boundary layer at $R = 570$ and $\omega = 0.1249$.

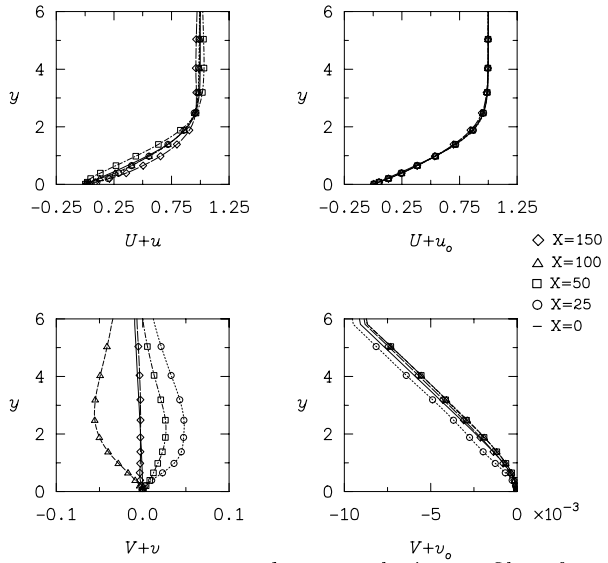

Fig. 4. Instantaneous and mean velocity profiles of nonlinear, subcritically growing disturbance in attachment-line boundary layer at $R = 570$ and $\omega = 0.1249$.

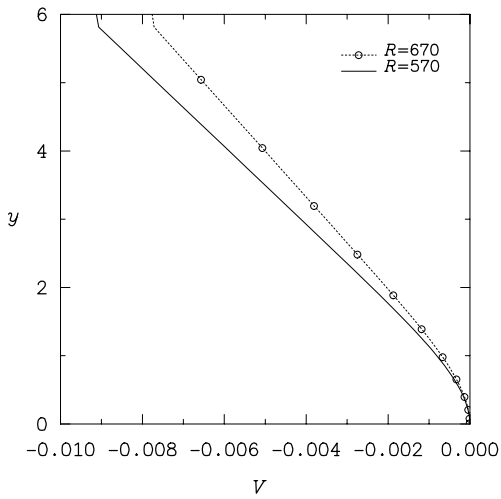

Fig. 5. Wall-normal component of base flows that corresponds to $R = 570$ and $R = 670$.

To control the subcritical growth of disturbances, various levels of suction are employed. Although Hall and Malik[9] note that suction makes the flow more susceptible to subcritical instability growth, Fig. 6 shows that this subcritical disturbance growth can be controlled by using small levels of suction. If the 2-D DNS results mimic the actual 3-D behavior of the flow, then large-amplitude disturbances generated on the attachment line can be controlled with suction.

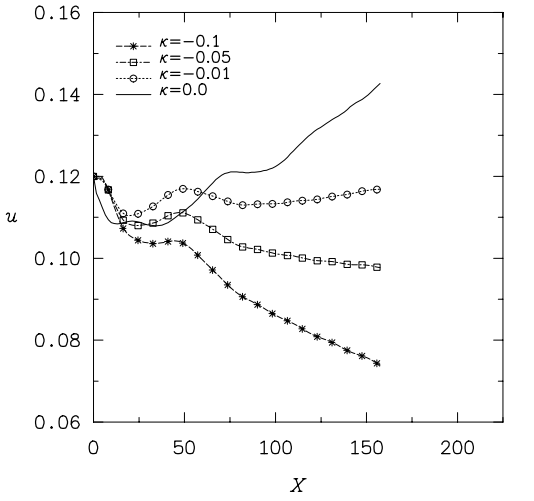

Fig. 6. Control of nonlinear subcritical disturbance growth in attachment-line boundary layer at $R = 570$ and $\omega = 0.1249$ with suction.

4.2 Linear & Nonlinear Instability at Upper Branch

Stability in the region near branch II of the neutral curve is studied. The disturbances are forced by suction and blowing at the wall with an amplitude of $A = 0.001$ percent. The growth and the decay of various frequency waves at $R = 684.2$ are shown in Fig. 7. Approximate growth rates are listed in the figure with a superimposed neutral solution (horizontal line). These results are in agreement with the neutral curve that was predicted theoretically by Hall et al.[8] The results also agree with a recent linear DNS study by Theofilis.[24]

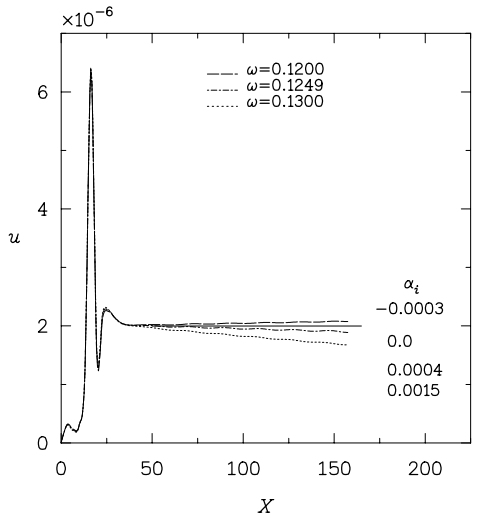

Fig. 7. Instability growth and decay near neutral curve of attachment-line boundary layer at $R = 684.2$.

The effect of both steady suction and steady blowing on linear instability growth in this region is documented. The amplification of a growing wave at $R = 684.2$ and $\omega = 0.1150$ is shown with the growth or decay of similar waves that evolve in swept Hiemenz flow in the presence of steady suction or blowing. The results indicate that suction stabilizes and blowing significantly destabilizes the disturbance. The effects of suction and blowing on disturbances computed by DNS are in agreement with the theory of Hall et al.[8] for small-amplitude disturbances.

To determine if nonlinear disturbance growth or equilibrium states can be found above branch II of the neutral stability curve and to ensure that the subcritical growth (obtained both by Hall and Malik[9] and the DNS shown in Fig. 3) did not artificially result from the disturbance forcing at the inflow boundary, a sequence of simulations was performed with harmonic-source generators at the wall. The disturbances are forced by suction and blowing at a decaying mode that corresponds to $R = 684.2$ and $\omega = 0.1249$. The initial amplitudes of the disturbances for each simulation were incrementally increased until the otherwise linearly decaying mode became amplified because of the nonlinear forcing. With steady suction, the results further demonstrate that small amounts of suction can be used to stabilize these disturbances. To study the subcritical growth phenomenon, Theofilis[15] used suction and blowing to initiate disturbances in the simulations. It is clear from the present results that Theofilis[15] failed to obtain subcritical growth because the suction and blowing amplitudes were too small to generate a subcritically growing disturbance.

The simulations are repeated for the mode that corresponds to $R = 684.2$ and $\omega = 0.1230$, which is closer to branch II of the neutral curve. The results indicate that nonlinear growth can be obtained from disturbances with smaller initial amplitudes. As expected, smaller amounts of suction are required to stabilize the disturbances. This series of simulations was conducted to demonstrate nonlinear growth close to branch II of the neutral curve; these results create a foundation for 3-D nonlinear simulations. Because significant computational cost is involved with 3-D simulations and because the forcing of disturbances with very large initial amplitudes requires more grid resolution, these 2-D simulations have established that forcing smaller amplitude disturbances close to branch II will yield nonlinearly growing modes. Furthermore, smaller amounts of suction can be used to stabilize these growing modes.

4.3 Linear & Nonlinear Instability at Lower Branch

Finally, the region near branch I of the neutral curve is studied. The evolution of disturbances generated by suction and blowing at $R = 684.2$ and $\omega = 0.0840$ is shown in Fig. 8. For small-amplitude disturbances, the theory of Hall et al.[8] give slightly different results compared with both the present DNS results and the DNS results of Theofilis.[24] Because the relative errors between the theory and DNS frequencies are only 1 to 2 percent, the preditions of Hall et al.[8] for the instability characteristics are correct for practical applications. Various large-amplitude disturbances were forced by suction and blowing; no subcritical growth was detected near branch I of the neutral curve. However, supercritical large-amplitude disturbances approach a state that agrees with Hall and Malik.[9] Furthermore, this equilibriumlike state agrees with the experimental observations of Pfenninger and Bacon.[5]

5. Three-Dimensional Simulation Results

The 3-D simulations are performed on a grid of 661 points along the attachment line, 81 points in the wall-normal direction, and 25 points in the flow-acceleration

direction. The far-field boundary is located at 50δ from the wall, the computational length along the attachment line is 216.56δ, and the flow-acceleration boundaries are located $\pm 100\delta$ from the attachment line. For the time-marching scheme, the disturbance wavelength was divided into 320 time steps per period. The total Cray Y-MP time for a simulation with a single processor was approximately 25 hrs (with a single processor).

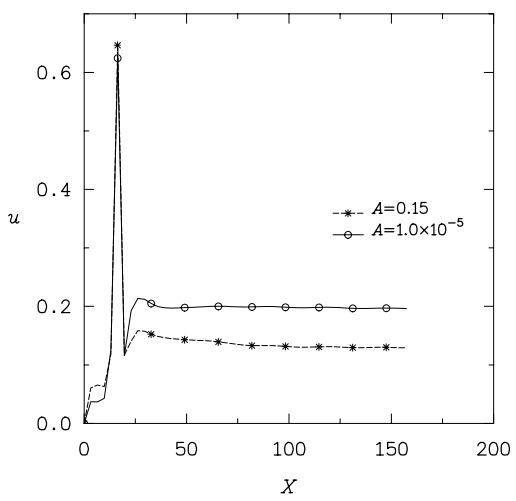

Fig. 8. Linear decay and nonlinear equilibrium in attachment-line boundary layer at $R = 684.2$ and $\omega = 0.0840$. (Disturbances normalized by initial amplitudes.)

5.1 Region of Disturbance Decay

The nonparallel theory of Hall et al.[8] outlined the stable and unstable regions for infinitesimal disturbances. In a segment of the subcritical region, large-amplitude disturbances were found by Hall and Malik[9] to exhibit nonlinear amplification. The 2-D DNS results confirmed this subcritical growth phenomenon. In this section, the Reynolds number $R = 570$ and the frequency $\omega = 0.1249$, which are parameters in the subcritical region, are used in the study of the evolution of small-amplitude 3-D disturbances. The results are compared with LST and the 2-D DNS results.

To compare with the 2-D results, a quasi-2-D disturbance is initiated in the 3-D flow. At best, this disturbance is an approximation to a true 2-D instability. To generate this 2-D disturbance, a harmonic source is used that is elongated ($-44.2 < Z < 44.2$) in the flow-acceleration direction. This disturbance-forcing method is comparable to using a vibrating ribbon to generate 2-D disturbances for wind-tunnel experiments. The qualitative features of a disturbance generated by the harmonic source with a small amplitude (e.g., $A = 0.001$ percent) are shown in Fig. 9. The disturbance evolution is viewed from above and along the attachment line. The wave travels along the attachment line without significant 3-D features. However, because the base flow is accelerating away from the attachment line (in the $\pm Z$ directions), wave spreading occurs with distance from the harmonic source, and the rate of spreading increases with distance along the attachment line.

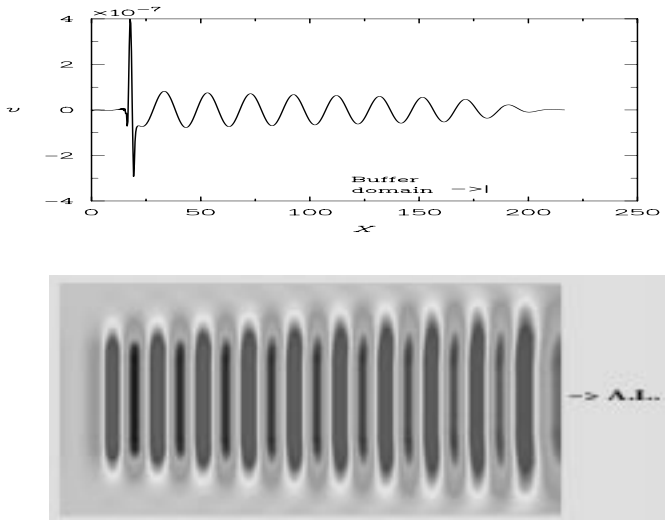

Fig. 9. Side and top view of 3-D traveling wave in attachment-line boundary layer.

The quasi-2-D simulation results for both a quasi-parallel base flow (i.e., $V = 0$) and the full swept Hiemenz flow were compared with linear stability theory. The amplitude, decay rate, and wavelength of disturbances simulated with the quasi-parallel flow are in excellent quantitative agreement with the 2-D LST results. This agreement suggests that in this parameter region the elongated harmonic source can approximate a 2-D disturbance on the attachment line. Similar to the 2-D DNS comparison, the full swept Hiemenz base flow destabilizes disturbances due to the inclusion of the V velocity component. This destabilizing feature is consistent with theory.

To further demonstrate the 2-D nature of the disturbance generated with the elongated harmonic source, Fig. 10 shows the attachment-line results compared with results at a distances 13δ and 35δ off the attachment line. The evolution patterns are identical out to near 35δ, where small deviations are observed. This implies that the elongated harmonic source is generating primarily 2-D waves and that the attachment-line velocity component is dominant (i.e., the amplitude of the w velocity component of the disturbance is too small to modify the dominant u component). The u and w

velocity profiles at $Z = 13\delta$ and 35δ reveal only small differences with u velocity components and large differences with w velocity components. The w velocity is an order of magnitude smaller than the u velocity, which is the reason for the good agreement between the u velocity on the attachment line with the same components off the attachment line. Furthermore, although no symmetry assumption is made, flow symmetry about the attachment line is realized with this particular harmonic-source generator.

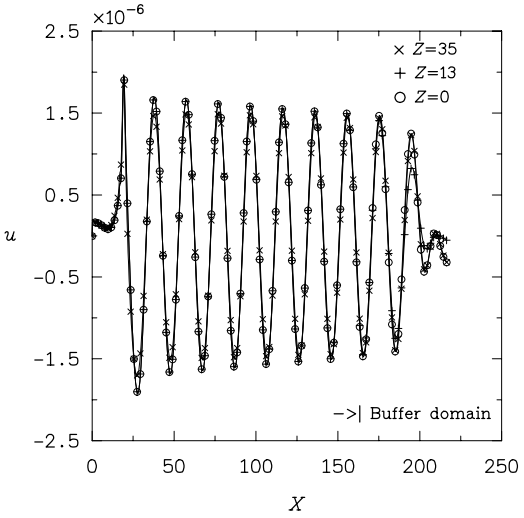

Fig. 10. Flow-acceleration variation of simulated 2-D disturbance evolution in 3-D attachment-line base flow for $R = 570$ and $\omega = 0.1249$.

In Figs. 11 and 12, 3-D simulation results on the attachment line are compared with previous 2-D DNS results. Figure 11 clearly shows a significant amplitude disparity between the 2-D and 3-D results. Because the 3-D simulations contain a flow-acceleration velocity component w, an additional degree of freedom is available to disperse (or absorb) energy. Hence, the harmonic-source generator forces less energy into the attachment-line velocity component u. The 2-D and 3-D results (normalized by the 2-D maximum of the u velocity) are also shown in Fig. 11 to enable a growth-rate comparison. The disturbance is slightly more destabilized in the full 3-D flow than in the 2-D flow approximation. Similar qualitative differences are evident when disturbance growth rates in quasi-parallel flow are compared with those in nonparallel flows. Finally, normalized primary wave velocity profiles are compared in Fig. 12. The shapes of the compared profiles agree well. The results demonstrate that 2-D simulations capture the qualitative features of the true 3-D flow; in addition, because a third degree of freedom (w, z) is not present in the 2-D simulations, amplitude information is overpredicted, and growth-rate information is underpredicted. These results suggest that much larger disturbances will be required to generate subcritical disturbance growth in the 3-D flow (if subcritical growth is possible in the 3-D flow).

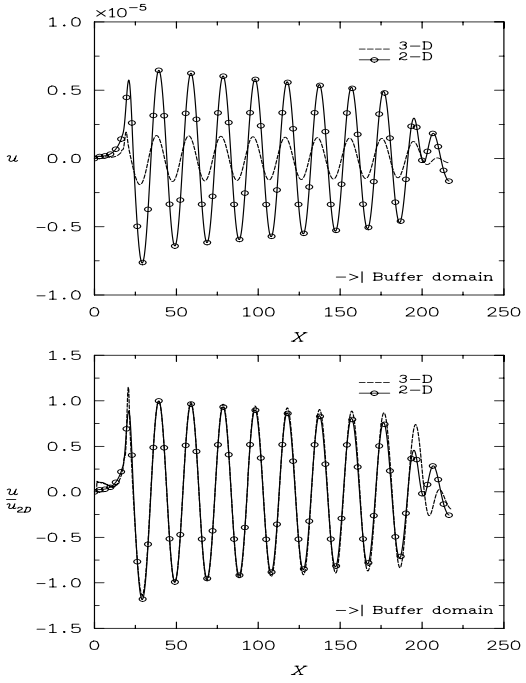

Fig. 11. Comparison of 2-D and 3-D disturbance evolutions in 3-D attachment-line boundary layer for $R = 570$ and $\omega = 0.1249$.

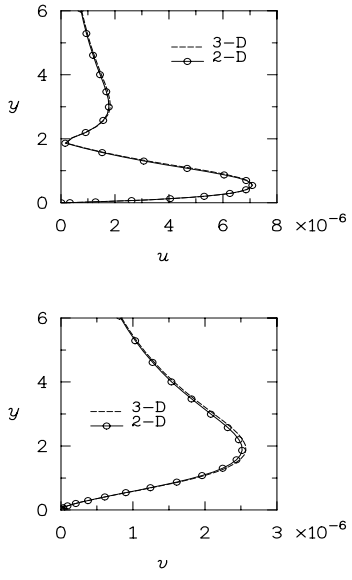

Fig. 12. Comparison of normalized 2-D and 3-D primary wave velocity profiles at $X = 100$ in attachment-line boundary layer at $R = 570$ and $\omega = 0.1249$.

In the nonparallel theory of Hall et al.[8], the z-dependent form for the flow-accelerated velocity component w was a key assumption, which led to a system of ordinary differential equations rather than partial differential equations. Figure 13 shows the maximum amplitudes of the flow-accelerated velocity component at $X = 100$ with distance from the attachment line. For the present harmonic source, this z-dependent disturbance form assumed by Hall et al.[8] is realized in the simulation near the attachment line; however, because the harmonic source has a finite length, the disturbance behavior near the harmonic-source ends deviates from the assumed z dependence. The harmonic-source ends cause a perturbation to the flow. Similar difficulties in disturbance initialization can be found in the experiments; however, the core of the test region (i.e., the attachment line) is not significantly contaminated by these end effects.

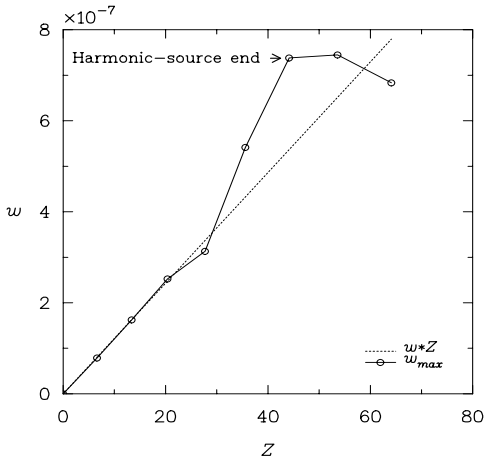

Fig. 13. Maximum flow-accelerated disturbance velocity w with distance from attachment line at $X = 100$, $R = 570$, and $\omega = 0.1249$.

In the next section, the simulation results are presented for the neutral-curve regions described by the nonparallel theory of Hall et al.[8]

5.2 The Neutral-Curve Region

In parameter regimes near the neutral curve, finite Reynolds number instabilities are studied near the upper branch, the lower branch, and the critical point to locate the neutral curve. The harmonic-source disturbance generator is used to generate the 2-D modes on the attachment line.

For the Reynolds number $R = 684.2$, the 3-D simulations yield an upper branch mode for the frequency $\omega = 0.1263$; the nonparallel theory of Hall et al.[8] and the 2-D DNS results indicate that the upper branch is between $\omega = 0.1230$ and $\omega = 0.1240$. Although the 2-D and 3-D results yield different upper branch locations, the relative error, or difference, in the locations is only about 2 percent. This difference may be attributed to the assumption that a 2-D disturbance is generated from a 3-D harmonic source or that the 3-D base flow does not support pure 2-D disturbances.

Near the critical-point region, digitized data from the results of Hall et al.[8] indicate that the Reynolds number $R = 580$ and frequency $\omega = 0.1104$ is the point furthest upstream at which an infinitesimal 2-D disturbance becomes unstable. Although this value is not the exact critical point, this Reynolds number and frequency combination lies on the neutral curve in the region of the critical point. The 3-D simulation results suggest that for the frequency $\omega = 0.1104$, the Reynolds number for neutral stability is slightly greater than $R = 585$. This leads to less than a 1-percent difference between the nonparallel theory and the simulation results.

Finally, simulations are performed near the lower branch of the neutral curve. The results indicate that for the Reynolds number $R = 684.2$ the lower branch of the neutral curve is approximately at the frequency $\omega = 0.082$, which agrees with nonparallel theory.

For practical engineering purposes, the nonparallel theory of Hall et al.[8] agrees with the 3-D DNS results in the limit of infinitesimal quasi-2-D disturbances that propagate along the attachment line.

5.3 Three-Dimensional Disturbances

To generate 3-D disturbances, the flow-acceleration length of the harmonic-source generator is reduced to enable a more direct transfer of energy to the w velocity component. Disturbances computed in the parameter regime described by a Reynolds number $R = 570$ and frequency $\omega = 0.1249$ are shown in Fig. 14. By reducing the length of the original harmonic source from $-44.2 < Z < 44.2$ to $-20.4 < Z < 20.4$, the generated disturbance is very similar to the previous quasi-2-D disturbance. However, by reducing the harmonic-source length to $-13.4 < Z < 13.4$ (one-third of the original length), the generated disturbance is significantly stabilized on the attachment line. The evolution no longer represents a quasi-2-D disturbance and becomes more comparable to a harmonic point source. Two-dimensional instabilities are apparently dominant on the attachment line.

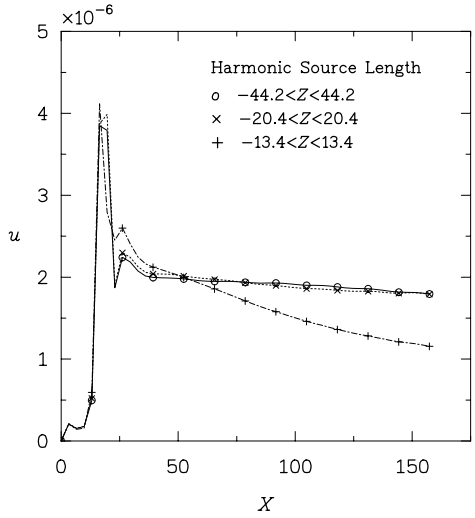

Fig. 14. Evolution of disturbances in attachment-line boundary layer at $R = 570$ and $\omega = 0.1249$, where disturbances are generated with harmonic sources of various lengths.

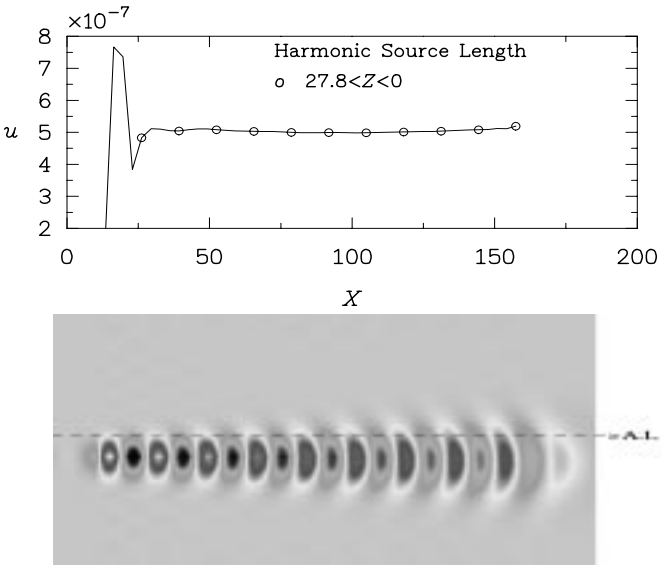

Fig. 15. Evolution of disturbance velocity u on attachment line and top view of 3-D traveling wave in attachment-line boundary layer at $R = 570$ and $\omega = 0.1249$.

Next, a harmonic-source generator is used to introduce a disturbance off the attachment line to determine the direction and rate of instability growth or decay. The results of a disturbance generated with a harmonic source located at $27.8 < Z < 0$ are shown in Fig. 15. The top view indicates that the harmonic source generates a disturbance that evolves along the attachment line with spreading both away from and toward the attachment line. These results suggest that the flow-accelerated shear away from the attachment line has insufficient strength to deter the spreading of the disturbance toward the attachment line. Figure 15 also shows that the maximum-amplitude u velocity on the attachment line initially undergoes a slight decay and then continues to grow. The amplitude informattion along the attachment line alone indicates an unstable mode in the simulations; however, the top view of the flow field indicates that this amplification is caused by the wave-spreading phenomenon. The combined amplitude and visual results imply that a disturbance generated off (but near) the attachment line can supply energy to the attachment region by the spreading of the wave pattern. In turn, this energy supply may feed an unstable mode on the attachment line.

For the final simulation in this subsection, the Reynolds number $R = 684.2$ and the frequency $\omega = 0.1150$ are used because nonparallel theory predicts that infinitesimal 2-D disturbances are unstable on the attachment line. The disturbance is generated with a harmonic source that is positioned at $35.6 < Z < 6.6$ (i.e., completely off the attachment line). The top view of the computed disturbance is shown in Fig. 16. The harmonic source has generated a disturbance with a circular pattern. As before, the disturbance evolves primarily along the attachment line, and the wave spreads both away from and toward the attachment line. The amplitude of the disturbance at various Z locations is shown in Fig. 17. The disturbance has a peak amplitude at initiated at $Z = 20.4$ and undergoes a strong decay along the attachment line, although the mode is predicted to be unstable on the attachment line. The spread of the disturbance toward the attachment line indicates that the disturbance on the attachment line is either unstable or merely gaining energy at a rate comparable to the spreading rate. However, because the theory for 2-D disturbances indicates that the disturbance is unstable on the attachment line, some combination of energy transfer due to spreading and linear growth is likely. However, the more stable 3-D modes may rob the 2-D mode of energy and prevent flow transition along the attachment line. Note that the u velocity components at all Z locations indicate increased amplitudes with along the attachment line, except for the $Z = 20.4$ location which indicates decay. Spreading causes the other Z locations

to receive energy, but because the $Z = 20.4$ location was the location of maximum initial amplitude and because the disturbance propagates along and away from the attachment line, the location of the maximum velocity is no longer at $Z = 20.4$. This results in an observed decay at the $Z = 20.4$ station. Figure 18 shows velocity profiles at various Z locations at $X = 100$. As energy is transferred because of this spreading, the profiles near the attachment line undergo a distortion near the wall. This distortion leads to multiple maximums and profile shapes that deviate from the linear theory.

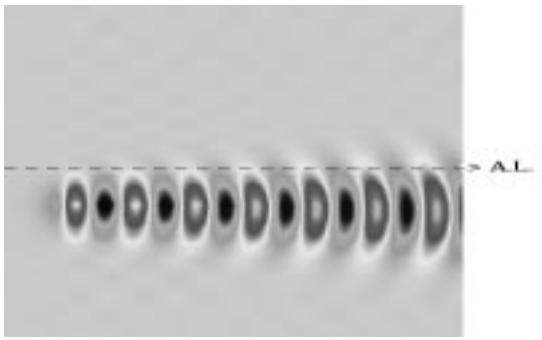

Fig. 16. Top view of disturbance evolution in attachment-line boundary layer at $R = 684.2$ and $\omega = 0.1150$, where disturbance is generated with harmonic source near attachment line.

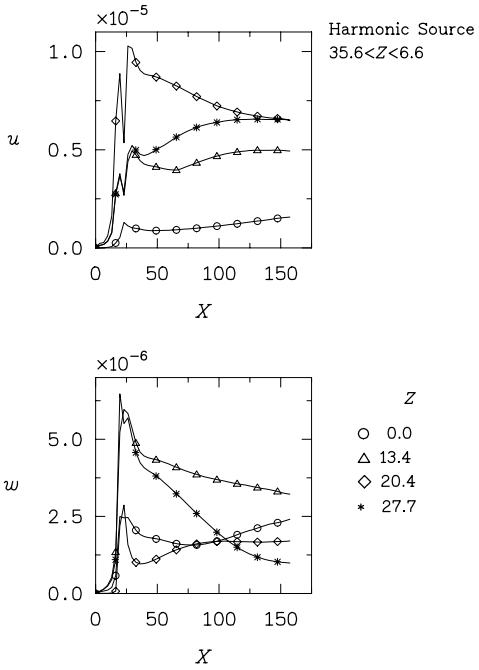

Fig. 17. Evolution of disturbance generated off attachment line in attachment-line boundary layer at $R = 684.2$ and $\omega = 0.1150$.

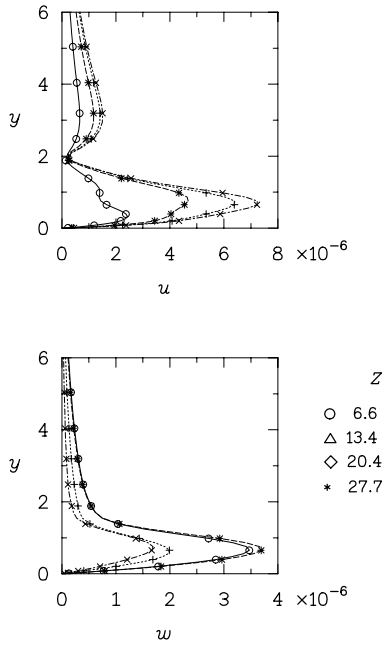

Fig. 18. Comparison of 3-D disturbance velocity profiles at $X = 100$ near attachment line at $R = 684.2$ and $\omega = 0.1150$.

5.4 Suction and Blowing Effects

By changing the boundary conditions in equation (7) from $\kappa = 0$, steady suction ($\kappa < 0$) or blowing ($\kappa > 0$) can be used to alter the growth or decay of disturbances in the attachment-line boundary-layer flow. Near the upper branch of the neutral curve, the Reynolds number $R = 684.2$ and frequency $\omega = 0.1230$ are used for the simple test case of linear stability with suction and blowing. The results of the quasi-2-D disturbance generated with the elongated harmonic source ($-44.2 < Z < 44.2$) indicate that suction stabilizes and blowing destabilizes the disturbance, which agrees with the theoretical results by Hall et al.[8] and the 2-D DNS results.

The results for the 3-D disturbance generated with a harmonic source of length $35.6 < Z < 6.6$ at the Reynolds number $R = 684.2$ and frequency $\omega = 0.1150$ indicated growth in the energy on the attachment line (Figs. 16 and 17). Because 2-D disturbances that correspond to this Reynolds number and frequency are linearly unstable on the attachment line, the presence of energy should lead to instability growth. Computations with suction are used to stabilize the disturbance on and near the attachment line. Clearly, Fig. 19 shows that suction stabilizes the disturbances located both on and off the attachment line.

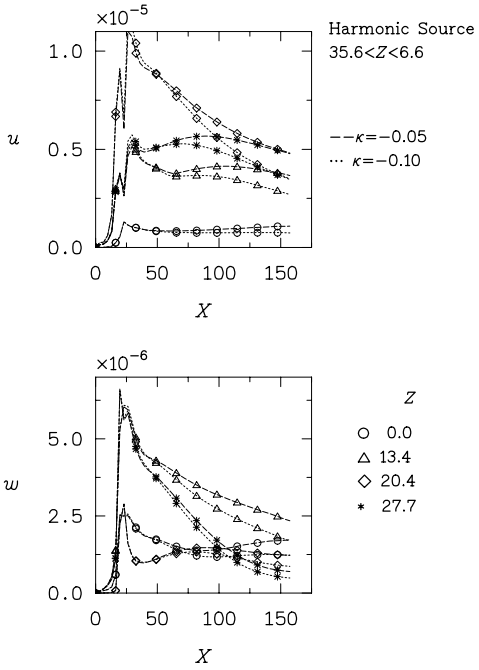

Fig. 19. Effect of suction on evolution of disturbance generated off attachment line in attachment-line boundary layer at $R = 684.2$ and $\omega = 0.1150$.

6. Concluding Remarks

In this paper, the results of two- (2-D) and three-dimensional (3-D) spatial direct numerical simulations (DNS) of attachment-line instabilities in swept Hiemenz flow are presented. With a quasi-parallel base flow approximation, the small-amplitude disturbances were shown to grow and decay in agreement with linear stability theory. The true swept Hiemenz base flow leads to a destabilization of the disturbances, which agrees with the nonparallel theory of Hall et al.[8] Furthermore, the effect of steady suction and blowing on small-amplitude disturbances was evaluated with DNS. In agreement with the results of Hall et al.,[8] suction stabilizes and blowing destabilizes small-amplitude disturbances.

Subcritical instability growth was detected with the weakly nonlinear theory of Hall and Malik[9] and later refuted with 2-D DNS results by Jiménez et al.[14] Theofilis.[15] Although it is clear that Theofilis[15] did not obtain subcritical growth because the initial disturbance amplitudes were too small, it is not clear why Jiménez et al.[14] failed to obtain subcritical growth. The present simulations have found subcritical instability growth and confirm the former theoretical results of Hall and Malik[9]. We surmise that (similar to nonparallel effects) nonlinear disturbances broaden the neutral curve toward higher frequencies in the critical region. Furthermore, the DNS results demonstrate that small amounts of steady suction stabilize the otherwise subcritically growing disturbances.

The neutral-curve location predicted by the nonparallel theory of Hall et al.[8] agreed well with the 3-D simulation results in the limit of the infinitesimal 2-D disturbances, that propagate along the attachment line.

For the parameter regions studied here, instabilities that are generated from harmonic sources located off the attachment line spread both toward and away from the attachment line. Because of this spreading, energy from the initial disturbance is transferred to the attachment-line instabilities; however, suction stabilizes these instabilities. Furthermore, 3-D instabilities were more stable than 2-D or quasi-2-D instabilities.

Acknowledgments

The author wishes to express his gratitude to Drs. Bart A. Singer and Craig L. Streett for reviewing this manuscript and for providing useful comments to enhance the final draft. Also, thanks goes to Ms. Jonay A. Campbell for her editorial assistance.

References

1. Gaster, M., "A Simple Devise for Preventing Turbulent Contamination on Swept Leading Edges," *J. Roy. Aero. Soc.*, Vol. 69, 1965, pp. 788-789.

2. Pfenninger, W., Laminar Flow Control -Laminarization. AGARD-R-654, 1977.

3. Gaster, M., "On the Flow Along Swept Leading Edges," *The Aeronautical Quarterly*, Vol. 18, 1967, pp. 165-184.

4. Cumpsty, N. A. and Head, M. R., "The Calculation of the Three-Dimensional Turbulent Boundary Layer. Part III. Comparison of Attachment-Line Calculations with Experiment," *The Aeronautical Quarterly*, Vol. 20, 1969, pp. 99-113.

5. Pfenninger, W. and Bacon, J. W., Jr., "Amplified Laminar Boundary-Layer Oscillations and Transition at the Front Attachment Line of a 45^o Swept Flat-Nosed Wing With and Without Boundary-Layer Suction," *Viscous Drag Reduction*, (C. S. Wells, ed.), Plenum Press, 1969, pp. 85-105.

6. Poll, D. I. A., "Transition in the Infinite Swept Attachment Line Boundary Layer," *The Aeronautical Quarterly*, Vol. 30, 1979, pp. 607-628.

7. Poll, D. I. A., "Three-Dimensional Boundary Layer Transition Via the Mechanisms of Attachment-Line Contamination and Crossflow Instability," *Laminar-Turbulent Transition*, (R. Eppler and H. Fasel, eds.), Springer-Verlag: Stuttgart, 1980, pp. 253-262.

8. Hall, P., Malik, M. R., and Poll, D. I. A., "On the Stability of an Infinite Swept Attachment Line Boundary Layer," *Proceedings of the Royal Society of London*, Vol. A395, 1984, pp. 229-245.

9. Hall, P. and Malik, M. R., "On the Instability of a Three-Dimensional Attachment-Line Boundary Layer: Weakly Nonlinear Theory and a Numerical Simulation," *J. Fluid Mech.*, Vol. 163, 1986, pp. 257-282.

10. Hall, P. and Seddougui, S. O., "Wave Interactions in a Three-Dimensional Attachment-Line Boundary Layer," *J. Fluid Mech.*, Vol. 217, 1990, pp. 367-390.

11. Spalart, P. R., "Direct Numerical Study of Leading-Edge Contamination," AGARD-CP-438, 1989, pp. 5.1-5.13.

12. Joslin, R. D., Streett, C. L., and Chang, C.-L., "Validation of Three-Dimensional Incompressible Spatial Direct Numerical Simulation Code—a Comparison with Linear Stability and Parabolic Stability Equations Theories for Boundary-Layer Transition on a Flat Plate," NASA TP-3205, 1992.

13. Joslin, R. D., Streett, C. L., and Chang, C.-L., "Spatial Direct Numerical Simulation of Boundary-Layer Transition Mechanisms: Validation of PSE Theory," Accepted for publication in *Theoretical and Computational Fluid Dynamics*, 1993.

14. Jiménez, J., Martel, C., Agüí, J. C., and Zufiria, J. A., "Direct Numerical Simulation of Transition in the Incompressible Leading Edge Boundary Layer," ETSIA/MF-903, 1990.

15. Theofilis, V., "A Spectral Velocity-Vorticity Algorithm for the Solution of the Incompressible Navier-Stokes Equations," *Numer. Methods in Laminar-Turbulent Flow*, (C. Taylor, ed.), Pineridge, 1993, pp. 801–811.

16. Hiemenz, K., "Die Grenzschicht an Einem in den Gleichförmigen Flüssigkeitsstrom Eingetauchten Geraden Kreiszylinder," Thesis, Göttingen 1911, *Dingl. Polytechn. J.*, Vol. 326, 1911, p. 321.

17. Canuto, C., Hussaini, M. Y., Quarteroni, A., and Zang, T. A., *Spectral Methods in Fluid Dynamics*, Springer-Verlag: New York, 1988.

18. Streett, C. L., and Hussaini, M. Y., "A Numerical Simulation of the Appearance of Chaos in Finite-Length Taylor-Couette Flow," *Appl. Numer. Math.*, Vol. 7, 1991, pp. 41-71.

19. Williamson, J. H., "Low-Storage Runge-Kutta Schemes," *J. Comput. Phys.*, Vol. 35, No. 1, 1980, pp. 48-56.

20. Danabasoglu, G., Biringen, S., and Streett, C. L., "Numerical Simulation of Spatially-Evolving Instability Control in Plane Channel Flow," AIAA Paper No. 90-1530, 1990.

21. Danabasoglu, G., Biringen, S., and Streett, C. L., "Spatial Simulation of Instability Control by Periodic Suction and Blowing," *Phys. Fluids* A, Vol. 3(9), 1991, pp. 2138-2147.

22. Lynch, R. E., Rice, J. R., and Thomas, D. H., "Direct Solution of Partial Difference Equations by Tensor Product Methods," *Num. Math.*, Vol. 6, 1964, pp. 185-199.

23. Streett, C. L. and Macaraeg, M. G., "Spectral Multi-Domain for Large-Scale Fluid Dynamic Simulations," *Int. J. Appl. Numer. Math.*, Vol. 6, 1989, pp. 123-140.

24. Theofilis, V., "Numerical Experiments on the Stability of Leading Edge Boundary Layer Flow: A Two-Dimensional Linear Study," *Int. J. Num. Methods in Fluids*, Vol. 16, 1993, pp. 153-170.